
Article:
Flintoft, Ian David, Bale, Simon Jonathan, Parker, Sarah et al. (2016) On the measureable range of absorption cross-section in a reverberation chamber. IEEE Transactions on Electromagnetic Compatibility. 7342957. pp. 22-29. ISSN: 0018-9375

https://doi.org/10.1109/TEMC.2015.2499841

On the Measurable Range of Absorption Cross-Section in a Reverberation Chamber

Ian D. Flintoft, Simon J. Bale, Sarah L. Parker, Andy C. Marvin, John F. Dawson and Martin P. Robinson

Department of Electronics, University of York, Heslington, York YO10 5DD, UK

Published in IEEE Transaction on Electromagnetic Compatibility

Accepted for publication 08/11/2015

DOI: 10.1109/TEMC.2015.2499841

URL: http://ieeexplore.ieee.org/stamp/stamp.jsp?tp=&arnumber=7342957&isnumber=4358749

On the Measurable Range of Absorption Cross-Section in a Reverberation Chamber

Ian D. Flintoft, *Senior Member, IEEE*, Simon J. Bale, *Member, IEEE*, Sarah L. Parker, Andy C. Marvin, *Fellow, IEEE*, John F. Dawson, *Member, IEEE* and Martin P. Robinson

***Abstract*—Average absorption cross-section can be measured in a reverberation chamber with an uncertainty estimated from the number of independent samples of the chamber transfer function taken during the measurement. However the current uncertainty model does not account the loading effect of the object being measured or the presence of non-stochastic energy in the chamber, as characterized by the Rician K-factor. Here the uncertainty model for the absorption cross-section measurements has been extended to include both of these effects for the case of stepped mechanical tuning with a paddle and frequency tuning. The extended uncertainty formula has been applied to predicting the range over which absorption cross-section measurements can be made with a defined relative uncertainty in a chamber of given geometry, using both simple models for the reverberation chamber and the measured quality-factor and K-factor. The model has been validated using measurements on a set of absorbing cubes of different sizes compared to Mie Series calculation on sphere of equivalent surface area. The extended error model is particularly utile for the design of reverberation chambers and experiments for absorption cross-section measurements across a wide range of application areas.**

***Index Terms*— absorption cross-section, reverberation chamber, Rician K-factor, uncertainty analysis.**

I. Introduction

The electromagnetic absorption cross-section (ACS) of an object, averaged over angles and electromagnetic field polarizations, can be determined in a reverberation chamber by measuring the average power transmission between two antennas with and without the object-under-test (OUT) present in the chamber [1][2][3]. The measurement operates by averaging the transmission between the antennas over an ensemble of independent field configurations obtained by tuning the cavity modes. Such average quantities are denoted by $\langle \ldots \rangle$. The tuning randomizes the multiple reflections in the chamber and results in a statistically well-defined average field at any point. The average ACS is defined as the ratio of the average power absorbed by the OUT, $\langle P^{\mathrm{a}} \rangle$, to the average power density, $\langle S \rangle$, incident upon it:

$$\langle \sigma^{\mathrm{a}} \rangle = \frac{\langle P^{\mathrm{a}} \rangle}{\langle S \rangle}. \quad (1)$$

The ability to accurately measure the average ACS of an object is useful in many application areas. In the realm of electromagnetic compatibility the power absorbed by objects inside shielding enclosures has a direct impact on the internal electromagnetic environment in which electronic circuits are housed and therefore on the susceptibility of the system to electromagnetic interference. This applies both at the scale of equipment enclosures and at the scale of large systems such as whole aircraft [4]. Average ACS is directly related to the average reflection coefficient of an object's surface and therefore to the material's electrical parameters. Measurement of ACS is therefore also useful for material characterization, particularly at high frequencies [2][5]. ACS is also very closely related to average whole-body specific absorption rate and has therefore recently been applied to the determination of human exposure to electromagnetic fields in diffuse environments [6][7].

Measurement of ACS in reverberation chambers was introduced by Carlberg et al [1]. The method follows directly from Hill's founding work on reverberant environments and has been developed by other authors in different application areas [8][2][3]. The statistical uncertainty in the ACS measurement approach was first analyzed by Carlberg et al, using a simple model based on a fixed number of independent samples of the field taken during the measurement [1]. This model is useful for estimating the uncertainty of the ACS of relatively low-loss objects (which cause a low perturbation of the chamber loading) in a reverberation chamber with negligible non-stochastic fields. When faced with designing an experiment to measure ACS over a large dynamic range in real chambers with significant non-stochastic fields a more accurate uncertainty model is desirable. Remley et al have recently developed an uncertainty model for the power transfer function in the chamber incorporating the non-stochastic fields [9]. In this paper we extend the ACS uncertainty model to account for chamber loading and non-stochastic effects when stepped mechanical tuning and frequency tuning are used, allowing more reliable chamber and experimental design for a required ACS measurement range.

This paper is organized as follows: In Section II we briefly review the theory of ACS measurement in a reverberation chamber. We then go on to develop a generalized uncertainty

Submitted for review 4th September 2015. This work was supported by Huawei Technologies Co. Ltd., Shenzhen, P. R. China under Contract YB2014090010.

I. D. Flintoft, S. J. Bale, S. Parker, A. C. Marvin, J. F. Dawson and M. P. Robinson are with the Department of Electronics, University of York, Heslington, York, YO10 5DD (e-mail: {ian.flintoft, simon.bale, slp504, andy.marvin, john.dawson,martin.robinson}@york.ac.uk).

model for the measurement in Section III. A set of validation objects are described in Section IV, which were measured using the methodology summarized in Section V. We present results from the uncertainty model and measurements in Section VI and finally conclude in Section VII.

II. ACS Measurement theory

The average power transfer function between two antennas in a reverberation chamber, denoted by G_{21}, is related to the average total ACS of the chamber and its contents, $\langle\sigma_{\mathrm{T}}^{a}\rangle$, by

$$G_{21} = \eta_1^{\mathrm{T}}\eta_2^{\mathrm{T}}\frac{\lambda^2}{8\pi}\frac{1}{\langle\sigma_{\mathrm{T}}^{a}\rangle}, \tag{2}$$

where η_i^{T} are the total radiation efficiencies of the two antennas and λ is the wavelength [1]. The power transfer function is typically determined from the scattering parameter between the two antenna ports as $G_{21} = \langle|S_{21}|^2\rangle$. The total radiation efficiencies of the antennas are given by the products of the dissipative radiation efficiencies due to ohmic and dielectric losses on the antennas (η_i^{rad}) and the reflection mismatch factors $\left(1-\left|S_{ii}^{\mathrm{FS}}\right|^2\right)$ of each antenna, where S_{ii}^{FS} denotes the free-space reflection coefficient of the antennas. If the radiation loss efficiencies are known to be close to unity it may be sufficient to approximate $\eta_i^{\mathrm{T}} \approx \left(1-\left|S_{ii}^{\mathrm{FS}}\right|^2\right)$ and account for the approximation in the systematic uncertainty estimate. The individual total antenna efficiencies can be determined using a three-antenna method in the reverberation chamber [10]. Note that the one and two antennas methods in [10] make assumptions about the back-scattering factor(s) at the antennas which may not be valid at high frequencies.

Since average ACS is additive within the assumptions of the ideal reverberation chamber model the ACS of the object-under-test (OUT), denoted by $\langle\sigma_{\mathrm{OUT}}^{\mathrm{a}}\rangle$, can be determined from measurements of the average chamber power transmission factor with and without the object present in the chamber as long as everything else is left invariant. Denoting the power transfer functions of the loaded and unloaded chamber by G_{21}^{loaded} and $G_{21}^{\mathrm{unloaded}}$ respectively the ACS of the OUT is given by [1]

$$\langle\sigma_{\mathrm{OUT}}^{\mathrm{a}}\rangle = \frac{\lambda^2}{8\pi}\eta_1^{\mathrm{T}}\eta_2^{\mathrm{T}}\left(\frac{1}{G_{21}^{\mathrm{loaded}}}-\frac{1}{G_{21}^{\mathrm{unloaded}}}\right). \tag{3}$$

III. Uncertainty Model

Carlberg et al deduced a formula for the 65 % confidence level relative uncertainty in the ACS measurement [1]

$$\frac{\Delta\langle\sigma_{\mathrm{OUT}}^{\mathrm{a}}\rangle}{\langle\sigma_{\mathrm{OUT}}^{\mathrm{a}}\rangle} \overset{\mathrm{def}}{\equiv} \alpha = \frac{\sqrt{2}L}{L-1}\frac{\mathrm{Var}[G_{21}]}{G_{21}} = \frac{\sqrt{2}L}{L-1}\frac{1}{\sqrt{N_{\mathrm{ind}}}}, \tag{4}$$

in terms of the number of uncorrelated samples of the field, N_{ind}, taken during the measurement and the chamber loading factor, L, defined by

$$L \overset{\mathrm{def}}{=} \frac{G_{21}^{\mathrm{unloaded}}}{G_{21}^{\mathrm{loaded}}} = 1 + \frac{\langle\sigma_{\mathrm{OUT}}^{\mathrm{a}}\rangle}{\langle\sigma_{\mathrm{unloaded}}^{\mathrm{a}}\rangle} \geq 1. \tag{5}$$

Here $\mathrm{Var}[G_{21}]$ is the variance of the power transfer function and $\langle\sigma_{\mathrm{unloaded}}^{\mathrm{a}}\rangle$ is the average absorption cross-section of the unloaded chamber. A simple model for the total ACS of the chamber, excluding the OUT is [8]

$$\langle\sigma_{\mathrm{unloaded}}^{\mathrm{a}}\rangle = \frac{4\pi}{3\lambda}\delta_s A + \eta_1^{\mathrm{T}}\frac{\lambda^2}{4\pi} + \eta_2^{\mathrm{T}}\frac{\lambda^2}{8\pi}, \tag{6}$$

where A is the total area of the chamber walls, $\delta_{\mathrm{s}} = 2/\sqrt{\omega\mu_0\sigma_{\mathrm{walls}}}$ is the skin depth and σ_{walls} is the conductivity of the wall material (assumed to be non-magnetic), ω is the angular frequency and μ_0 is the permeability of free-space.

Equation (4) assumes that the number of independent samples is independent of the chamber loading and does not account for systematic errors due to the presence of non-stochastic energy in the chamber. We therefore seek to generalize the formula to include these effects. We begin by applying the standard propagation of uncertainty formula (for uncorrelated uncertainties) to (3) obtaining

$$\alpha = \frac{1}{1/G_{21}^{\mathrm{loaded}}-1/G_{21}^{\mathrm{unloaded}}}\sqrt{\frac{\mathrm{Var}[G_{21}^{\mathrm{loaded}}]}{\left(G_{21}^{\mathrm{loaded}}\right)^4}+\frac{\mathrm{Var}[G_{21}^{\mathrm{unloaded}}]}{\left(G_{21}^{\mathrm{unloaded}}\right)^4}},$$

which using (5) can be reduced to

$$\alpha = \frac{L}{L-1}\sqrt{\frac{\mathrm{Var}[G_{21}^{\mathrm{loaded}}]}{\left(G_{21}^{\mathrm{loaded}}\right)^2}+\frac{1}{L^2}\frac{\mathrm{Var}[G_{21}^{\mathrm{unloaded}}]}{\left(G_{21}^{\mathrm{unloaded}}\right)^2}}. \tag{7}$$

For an ideal chamber the variances in the power transfer function are given by $\mathrm{Var}[G_{21}] = G_{21}^2/N_{\mathrm{ind}}$ [11]. Substituting this in the above we find

$$\alpha = \frac{L}{L-1}\sqrt{\frac{1}{N_{\mathrm{ind}}^{\mathrm{loaded}}(L)}+\frac{1}{L^2}\frac{1}{N_{\mathrm{ind}}^{\mathrm{unloaded}}}}, \tag{8}$$

where we have explicitly denoted the dependence of $N_{\mathrm{ind}}^{\mathrm{loaded}}$ on L. To obtain Carlberg et al's formula we simple set $N_{\mathrm{ind}}^{\mathrm{loaded}} = N_{\mathrm{ind}}^{\mathrm{unloaded}} = N_{\mathrm{ind}}$ in the above and assume that $\langle\sigma_{\mathrm{OUT}}^{\mathrm{a}}\rangle \ll \langle\sigma_{\mathrm{unloaded}}^{\mathrm{a}}\rangle$ so that $L \approx 1$. We now consider the generalization of the formula.

A. Effect of chamber loading

The number of independent samples of the field inside a reverberation chamber that are available from chambers and tuners of different sizes has been investigated by a number of authors including [12][13][14]. An estimate of the number of independent samples from mechanical tuning using a paddle of height h_{s} and radius r_{s} is given by [12]

$$N_{\mathrm{ind;MS}} = \begin{cases} C_{\mathrm{MS;large}}\dfrac{\langle Q\rangle V_{\mathrm{s}}}{V} & f < f_{\mathrm{c;MS}} \\ C_{\mathrm{MS;small}}\dfrac{\lambda\langle Q\rangle V_{\mathrm{s}}^{2/3}}{V} & f \geq f_{\mathrm{c;MS}} \end{cases}, \tag{9}$$

where $V_{\mathrm{s}} = \pi r_{\mathrm{s}}^2 h_{\mathrm{s}}$ is the effective paddle volume,

$$f_{\mathrm{c;MS}} = \frac{C_{\mathrm{MS;small}}}{C_{\mathrm{MS;large}}}\mathrm{c}_0 V_{\mathrm{s}}^{-1/3}, \tag{10}$$

c_0 is the speed of light and $\langle Q\rangle$ is the total average quality factor of the chamber. The empirically derived stirring efficiency coefficients are taken as $C_{\mathrm{MS;large}} = 0.5$ and $C_{\mathrm{MS;small}} = 2$. The number of independent samples available

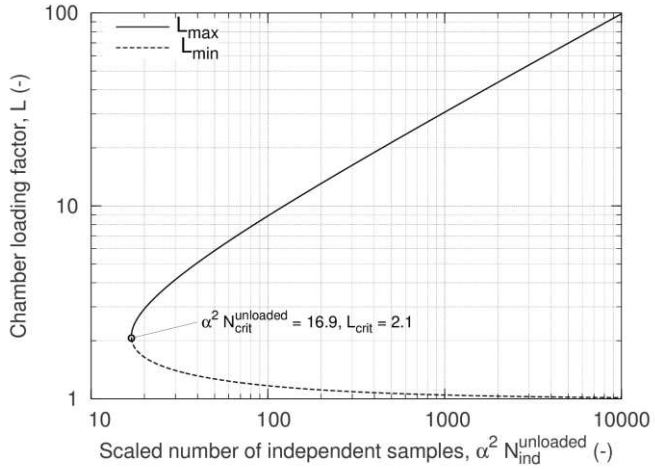

Fig. 1. Minimum and maximum chamber loading factor for ACS measurement with relative uncertainty less than α as function of the number of independent samples scaled by α^2.

from frequency stirring over a bandwidth Δf_{FS} can be estimated as [13]

$$N_{\mathrm{ind;FS}} = C_{\mathrm{FS}} \frac{\langle Q \rangle \Delta f_{\mathrm{FS}}}{f}, \tag{11}$$

where $C_{\mathrm{FS}} \approx 1$. The overall number of independent samples is the product of the numbers for mechanical and frequency tuning:

$$N_{\mathrm{ind}} = N_{\mathrm{ind;MS}} N_{\mathrm{ind;FS}} . \tag{12}$$

Note that in this paper we do not consider source stirring.

These studies show that, to first approximation, the number of independent samples available from both mechanical tuning and frequency tuning varies with the chamber total Q-factor and total ACS according to

$$N_{\mathrm{ind}} \propto \langle Q \rangle^2 \propto \frac{1}{\langle \sigma^{\mathrm{a}} \rangle^2} . \tag{13}$$

Using this relationship the number of independent samples is found to vary with the chamber loading factor according to

$$\frac{N_{\mathrm{ind}}^{\mathrm{unloaded}}}{N_{\mathrm{ind}}^{\mathrm{loaded}}} = \left(\frac{\langle \sigma_{\mathrm{unloaded}}^{\mathrm{a}} \rangle + \langle \sigma_{\mathrm{OUT}}^{\mathrm{a}} \rangle}{\langle \sigma_{\mathrm{unloaded}}^{\mathrm{a}} \rangle} \right)^2 = L^2 . \tag{14}$$

Substituting this into (8) the relative uncertainty in the ACS can be written

$$\alpha = \frac{L}{L-1} \sqrt{L^2 + \frac{1}{L^2}} \sqrt{\frac{1}{N_{\mathrm{ind}}^{\mathrm{unloaded}}}} . \tag{15}$$

This formula can be rearranged to give a quartic polynomial equation for the loading factor

$$L^4 - \alpha^2 N_{\mathrm{ind}}^{\mathrm{unloaded}} L^2 + 2\alpha^2 N_{\mathrm{ind}}^{\mathrm{unloaded}} L + 1 - \alpha^2 N_{\mathrm{ind}}^{\mathrm{unloaded}} = 0. \tag{16}$$

Introducing the scaled number of independent samples,

$$\tilde{\alpha}^2 = \alpha^2 N_{\mathrm{ind}}^{\mathrm{unloaded}}, \tag{17}$$

this can be written more concisely as

$$L^4 - \tilde{\alpha}^2 L^2 + 2\tilde{\alpha}^2 L + 1 - \tilde{\alpha}^2 = 0. \tag{18}$$

This equation determines the loading factors that give a relative uncertainty of α in the measured ACS of the OUT. The equation can be solved numerically and it is found that above a critical value of $\tilde{\alpha}_{\mathrm{crit}}^2 = \alpha^2 N_{\mathrm{ind;crit}}^{\mathrm{unloaded}} = 16.9$ there are two real solutions, $L_{\mathrm{min}}(\alpha^2 N_{\mathrm{ind}}^{\mathrm{unloaded}})$ and $L_{\mathrm{max}}(\alpha^2 N_{\mathrm{ind}}^{\mathrm{unloaded}})$, that determine the lower and upper bounds on L necessary for the relative uncertainty in the ACS to be less than α. Below the critical value, $\tilde{\alpha}^2 < \tilde{\alpha}_{\mathrm{crit}}^2 = 16.9$, there is no real solution of the quartic and it is not possible to measure the ACS with a relative uncertainty of α. At the critical point the loading factor is $L_{\mathrm{crit}} = 2.1$. The bounds on the loading factor as a function of $\tilde{\alpha}^2$ are shown in Fig. 1. The minimum and maximum ACS that can be measured with relative uncertainty α are related to the minimum and maximum loading factors by

$$\langle \sigma_{\mathrm{min/max}}^{\mathrm{a}} \rangle = \langle \sigma_{\mathrm{unloaded}}^{\mathrm{a}} \rangle \left(L_{\mathrm{min/max}} - 1 \right). \tag{19}$$

B. Effect of non-stochastic coupling

So far we have assumed that the field in the chamber is completely randomized and homogenized by multiple reflections. Real reverberation chambers also have some non-stochastic energy present. Formally, the chamber transmission factor (consider here to be the scattering parameter between the two antenna ports) can be decomposed into stochastic and non-stochastic parts, $S_{21} = S_{21}^{\mathrm{s}} + S_{21}^{\mathrm{ns}}$, where the vector average of the stochastic component $\langle S_{21}^{\mathrm{s}} \rangle = 0$ and hence $\langle S_{21} \rangle = \langle S_{21}^{\mathrm{ns}} \rangle$. The preponderance of non-stochastic energy is then quantified by the Rician K-factor defined by [15]

$$K = \frac{|S_{21}^{\mathrm{ns}}|^2}{\langle |S_{21}^{\mathrm{s}}|^2 \rangle} = \frac{|\langle S_{21} \rangle|^2}{\langle |S_{21} - \langle S_{21} \rangle|^2 \rangle} . \tag{20}$$

The K-factor is not an intrinsic property of the field in the chamber, but depends on the location and orientation of the antennas and other scattering objects within the chamber.

Remley et al have developed a model for the uncertainty in the reverberation chamber power transfer function that includes the effect of non-stochastic fields [9]. For the case where there is no source position tuning and the correlation function between the paddle angles is negligible the variance in the power transfer function is shown to be

$$\frac{\mathrm{Var}[G_{21}]}{G_{21}^2} = \frac{1}{N_{\mathrm{ind}}} + \frac{N_{\mathrm{ind}} - 1}{N_{\mathrm{ind}}} \left(\frac{K}{K+1} \right)^2 . \tag{21}$$

If $N_{\mathrm{ind}} \gg 1$ and $K \ll 1$ the second term related to the K-factor reduces to K^2, showing that the whole of the non-stochastic power is essentially regarded as an uncertainty in the power transfer function. Here we prefer to use this simpler approximation for the uncertainty contribution of the K-factor since it allows for a more straightforward calculation of the ACS uncertainty. Providing $N_{\mathrm{ind}} \geq 10$ and $K \leq 0.1$ the difference between the relative uncertainty predicted by the simplified and full formulas is less than 1 %. We therefore add terms $\mathrm{Var}[G_{21}]/G_{21}^2 = K^2$ for the both the loaded and unloaded chamber inside the surd in (8) to obtain

$$\alpha = \frac{L}{L-1} \sqrt{\frac{1}{N_{\mathrm{ind}}^{\mathrm{loaded}}} + K_{\mathrm{loaded}}^2 + \frac{1}{L^2} \left(\frac{1}{N_{\mathrm{ind}}^{\mathrm{unloaded}}} + K_{\mathrm{unloaded}}^2 \right)} . \tag{22}$$

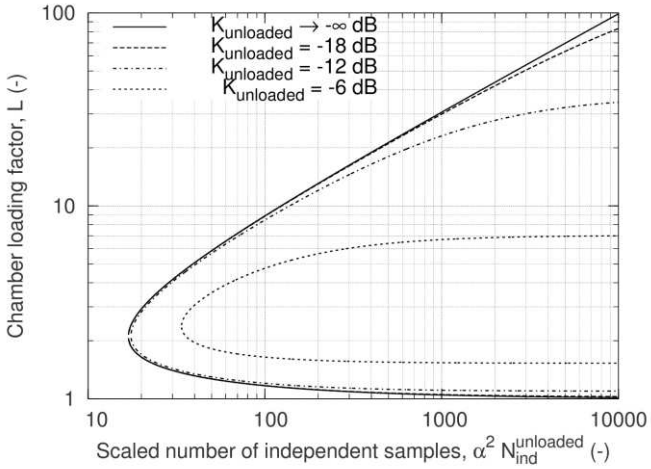

Fig. 2. Bounds on the chamber loading factor for an ACS measurement with relative uncertainty less than α as function of the number of independent samples and unloaded K-factor with $b = 2/5$.

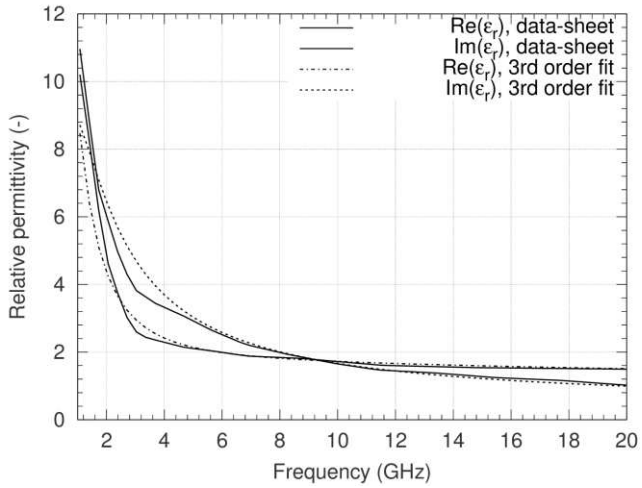

Fig. 3. Complex permittivity of the RAM used to fabricate the cubes, comparing the manufacturer's data to a third order Debye model.

This can be rearranged into

$$\alpha = \frac{L}{L-1}\frac{1}{\sqrt{N_{\text{ind}}^{\text{unloaded}}}}\cdot \sqrt{L^2 + \frac{1}{L^2} + N_{\text{ind}}^{\text{unloaded}} K_{\text{unloaded}}^2 \left(K_{\text{r}}^2 + \frac{1}{L^2}\right)}, \tag{23}$$

where the relative K-factor is defined by

$$K_{\text{r}} \overset{\text{def}}{\equiv} \frac{K_{\text{loaded}}}{K_{\text{unloaded}}}. \tag{24}$$

The K-factor generally increases with chamber loading, as the diffuse energy density inside the chamber is reduced by absorption in the load. A simple estimate for the K-factor in a chamber containing two antennas is [15]

$$K = \frac{3}{2}\frac{V}{\lambda\langle Q\rangle}\frac{D_1 D_2}{r_{12}^2}(\hat{\boldsymbol{\epsilon}}_1 \cdot \hat{\boldsymbol{\epsilon}}_2)^2, \tag{25}$$

where V is the chamber volume, D_1 and D_2 are the directivities of the transmitting and receiving antennas, r_{12} is the separation of the antennas and $(\hat{\boldsymbol{\epsilon}}_1 \cdot \hat{\boldsymbol{\epsilon}}_2)^2$ is the polarisation mismatch factor. In this model $K \propto 1/\langle Q\rangle \propto \langle \sigma^{\text{a}}\rangle$ and the relative K-factor

$$K_{\text{r}} = \frac{\langle \sigma_{\text{unloaded}}^{\text{a}}\rangle + \langle \sigma_{\text{OUT}}^{\text{a}}\rangle}{\langle \sigma_{\text{unloaded}}^{\text{a}}\rangle} = L \tag{26}$$

is numerically equal to the loading factor. Introducing this relationship into (23) we find that the uncertainty equation has same form as for the case without K-factor with the replacement

$$\alpha^2 N_{\text{ind}}^{\text{unloaded}} \rightarrow \frac{\alpha^2 N_{\text{ind}}^{\text{unloaded}}}{1 + N_{\text{ind}}^{\text{unloaded}} K_{\text{unloaded}}^2} \overset{\text{def}}{\equiv} \frac{\tilde{\alpha}^2}{1 + \tilde{K}_{\text{unloaded}}^2}. \tag{27}$$

Here we have introduced the scaled unloaded K-factor

$$\tilde{K}_{\text{unloaded}}^2 = N_{\text{ind}}^{\text{unloaded}} K_{\text{unloaded}}^2 \,. \tag{28}$$

Equation (26) is often found to overestimate the increase in K-factor with loading in realistic ACS measurement configurations [16]. A more general parametric model for the relative K-factor can be defined by

$$K_{\text{r}} = 1 + b(L-1) = 1 + b\frac{\langle \sigma_{\text{OUT}}^{\text{a}}\rangle}{\langle \sigma_{\text{unloaded}}^{\text{a}}\rangle}, \tag{29}$$

where $0 \le b \le 1$ is, for now, an empirically determined coefficient. When $b = 0$ the K-factor is independent of the chamber loading ($K_{\text{r}} = 1$), while if $b = 1$ we recover the simpler model in (26). This model is supported by the results in [16], which show that $K_{\text{r}} - 1 \propto \langle \sigma_{\text{OUT}}^{\text{a}}\rangle$. Substituting this into (8) we find, after some straightforward algebra, a modified quartic equation for the loading factor:

$$\left(1 + b^2\tilde{K}_{\text{unloaded}}^2\right)L^4 + 2b(1-b)\tilde{K}_{\text{unloaded}}^2 L^3 + \left(\tilde{K}_{\text{unloaded}}^2 - 2b\tilde{K}_{\text{unloaded}}^2 + b^2\tilde{K}_{\text{unloaded}}^2 - \tilde{\alpha}^2\right)L^2 + 2\tilde{\alpha}^2 L + 1 + \tilde{K}_{\text{unloaded}}^2 - \tilde{\alpha}^2 = 0. \tag{30}$$

This quartic reduces to (18) in the case $b = 0$ and $K_{\text{unloaded}} = 0$. The loading factor for a given relative uncertainty now depends on three parameters $L = L\left(\tilde{\alpha}^2, \tilde{K}_{\text{unloaded}}^2, b\right) = L\left(\alpha^2 N_{\text{ind}}^{\text{unloaded}}, K_{\text{unloaded}}^2 N_{\text{ind}}^{\text{unloaded}}, b\right)$. The bounds on the loading factor as a function of the unloaded K-factor for $b = 2/5$ (anticipating the measurement results in Section VI) are shown in Fig. 2. As the unloaded K-factor increases the critical point moves to higher values of $\tilde{\alpha}^2$ and the range of loading factors between the bounds reduces. As a guideline we find that an unloaded K-factor of about -10 dB represents the level of non-stochastic energy in the chamber at which the ability to measure ACS accurately starts to become seriously compromised.

IV. Validation Objects

In order to validate the uncertainty model, the ACSs of a family of different sized cubes constructed from radio absorbing material (RAM) were measured from 1 to 20 GHz. The properties of the cubes are defined in Table I. Each cube is identified by its side length in millimeters. The cubes were fabricated from commercially available carbon loaded

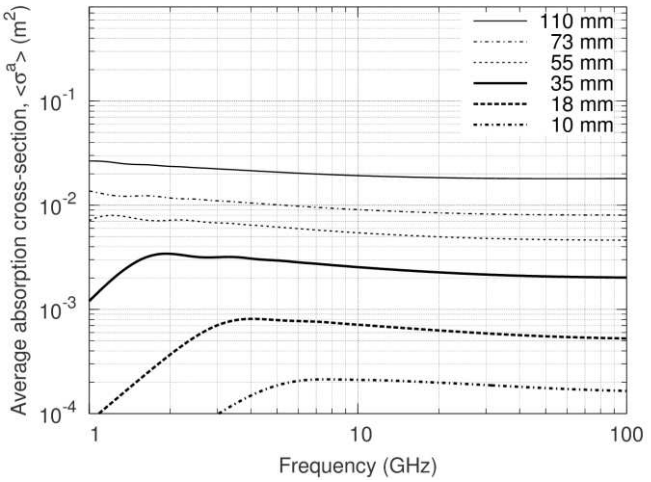

Fig. 4. ACS of the RAM cubes predicted by the Mie Series calculation for spheres of equivalent surface area.

TABLE I
PROPERTIES OF THE RAM CUBES

Side Length (mm)	Equivalent sphere radius (mm)
10	6.9
18	12.4
35	24.9
55	38.0
73	50.4
110	76.0

polyurethane foam RAM [17]. A three-pole Debye dispersion relationship

$$\hat{\varepsilon}_r = \varepsilon_\infty + \sum_{k=1}^{3} \frac{\Delta\varepsilon_k}{1+j\omega\tau_k} + \frac{\sigma_{DC}}{j\omega\varepsilon_0}, \quad (31)$$

was fitted to the manufacturer's complex permittivity data using a genetic algorithm. The parameters obtained were $\varepsilon_\infty = 1.1725$, $\Delta\varepsilon_1 = 1.04\times10^{-3}$, $\Delta\varepsilon_2 = 17.9$, $\Delta\varepsilon_3 = 0.490$, $\tau_1 = 55.3$ ms, $\tau_2 = 0.188$ ns, $\tau_3 = 6.20$ ps and $\sigma_{DC} = 0.1$ mS/m. The fitted complex permittivity is shown in Fig. 3, compared to the manufacturer's original data.

The ACS of each cube was predicted from a Mie Series solution for a sphere of the same surface area using the Debye model for the material permittivity [18]. The equivalent sphere radii are given in Table I. The ACSs predicted by the Mie Series are shown in Fig. 4; at the highest frequencies considered they span a two-decade range of ACS from about 2×10^{-4} m^2 to 2×10^{-2} m^2. For the smaller cubes the ACS falls at lower frequencies allowing the lower bound on the measurable ACS in the chamber to be probed. This behavior of the ACS is typical of most objects to which the measurement technique is applied. The working volume of the chamber used was not large enough to measure a cube with ACS near the upper bound on the measureable ACS.

V. MEASUREMENT METHODOLOGY

The RAM cubes were measured in a reverberation chamber with dimensions 0.6 m × 0.7 m × 0.8 m. The configuration of the chamber is shown in Fig. 5. The chamber was tuned using

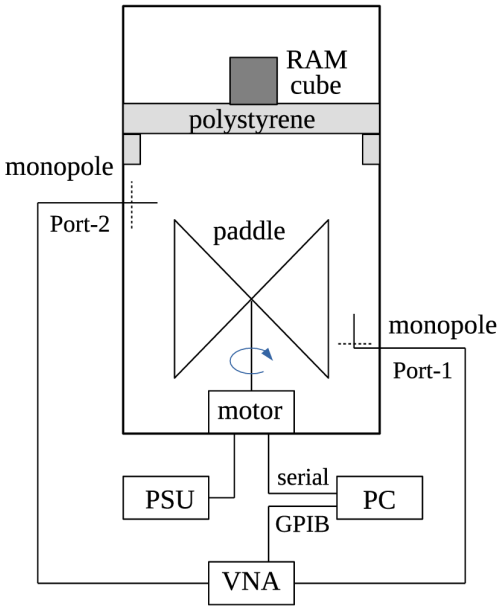

Fig. 5. Configuration of the reverberation chamber for the ACS measurements.

TABLE II
MEASUREMENT PARAMETERS

Parameter	Symbol	Value
Start frequency	f_{start}	1 GHz
Stop frequency	f_{stop}	20 GHz
Number of points	N_f	10,001
Frequency resolution	Δf	1.9 MHz
Sweep time	T_{sweep}	2.7 s
Number of paddle positions	N_{MS}	100
Frequency tuning bandwidth	Δf_{FS}	100 MHz

a mechanical paddle with height 0.30 m and radius 0.26 m and also by frequency tuning over a bandwidth of 100 MHz. The motor driving the paddle was powered from an external power supply unit (PSU) and controlled via a serial data-link. Both the power and data-link were made through multi-core shielded cables through a bulkhead connector in the chamber wall.

Two folded monopole antennas of length 40 mm and a vector network analyzer (VNA) were used to measure the chamber power transfer function. The two antennas were cross polarized and both were approximately 125 mm from the chamber wall. The dissipative radiation efficiencies of the monopoles were estimated from a circuit model and found to be greater than 0.97 over the measurement frequency range; they were therefore assumed to be unity [19].

The RAM cubes were placed on a rectangular expanded polystyrene base suspended above the paddle using expanded polystyrene mounts fixed to the side of the chamber wall. The parameters used for the ACS measurements are given in Table II. A full two-port calibration was carried out at the reference planes defined by the dashed lines in Fig 5.

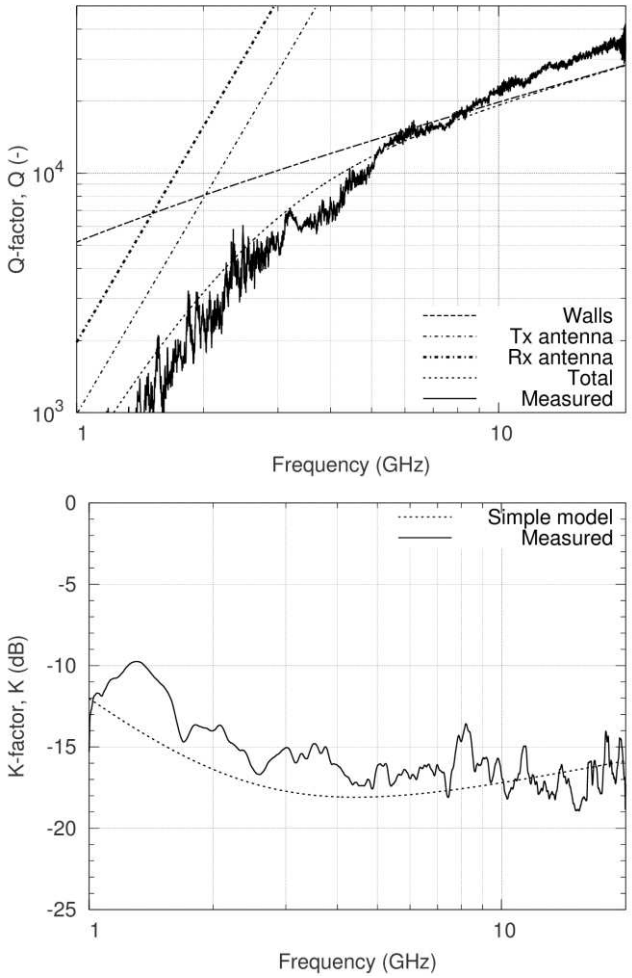

Fig. 6. Q-factor (top) and K-factor (bottom) of the unloaded chamber showing the measurement results compared to a semi-empirical model fitted to the measured data (using an effective wall conductivity of 0.35 MS/m).

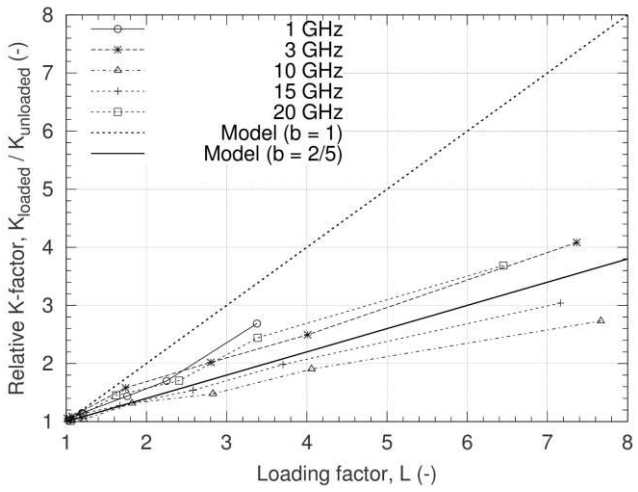

Fig. 7. Measured relative K-factor of the six RAM cubes in five different frequency bands as a function of the chamber loading factor. The simple parametric model with $b = 2/5$ provides a good estimate of the behavior.

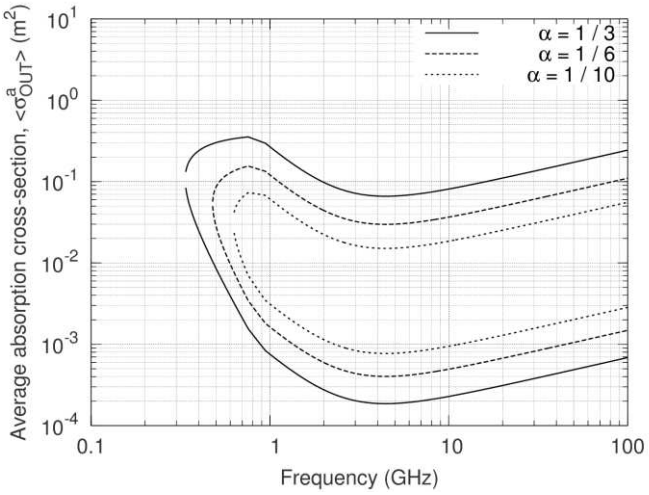

Fig. 8. Estimated boundaries on the ACS of an object for a relative uncertainty of $\alpha = 1/3$, 1/6 and 1/10 using the semi-empirical model for the chamber Q-factor and taking $K = 0$.

VI. Results

The measured Q-factor and K-factor of the unloaded chamber are shown in Fig. 6. The theoretical contributions of the antenna and wall losses to the Q-factor are also shown. The wall contribution was estimated by fitting the high frequency ACS of the chamber to the model in (6); an effective conductivity of 0.35 MS/m gave the best least-squares fit to the measured data. The antennas are the dominant loss mechanism below 2 GHz and have a significant effect up to 7 GHz. The measured K-factor is compared to the prediction of the model in (24) taking indicative directivities of 3.3 (the theoretical quarter-wave directivities, corresponding to a frequency of 2 GHz) for the two monopole antennas. The actual directives are both frequency and geometry dependent and also depend on scattering from the tuning paddle.

The measured relative K-factors of the chamber loaded with the different sized RAM cubes are shown in Fig. 7 as a function of the chamber loading factor for a number of frequencies. The results are consistent with the single parameter model proposed in (29) with $b \approx 2/5$, though the parameter does vary a little with frequency. Significantly, we see that taking $b = 1$ overestimates the increase in the K-factor with the chamber loading factor.

If the K-factor is taken to be negligible then the estimated bounds on the ACS for relative uncertainties of 1/3, 1/6 and 1/10 are shown in Fig. 8. This prediction uses the solution of (18) and the empirical models (9) and (10) to estimate the number of independent samples in the chamber. Above 1 GHz the 1/3 relative uncertainty range spans over two-decades; however, the location of the range varies as a function of frequency. Below 1 GHz the uncertainty bounds rapidly come together.

Including a loading independent K-factor ($b = 0$) in the uncertainty model using (30) results in the 1/3 relative uncertainty bounds shown in Fig. 9. As the K-factor increases the uncertainty bounds close in on each other and the critical point moves higher in frequency. Notably, the lower bounds are more strongly affected than the upper bound. With a K-factor of -6 dB the usable measurement range is very limited.

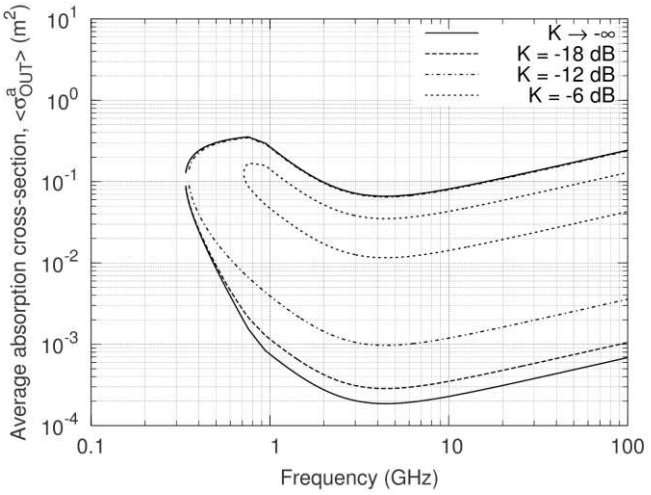

Fig. 9. Estimated boundaries on the ACS of an object for a relative uncertainty of α = 1/3 and various loading independent K-factors (b = 0) using the semi-empirical model for the chamber Q-factor.

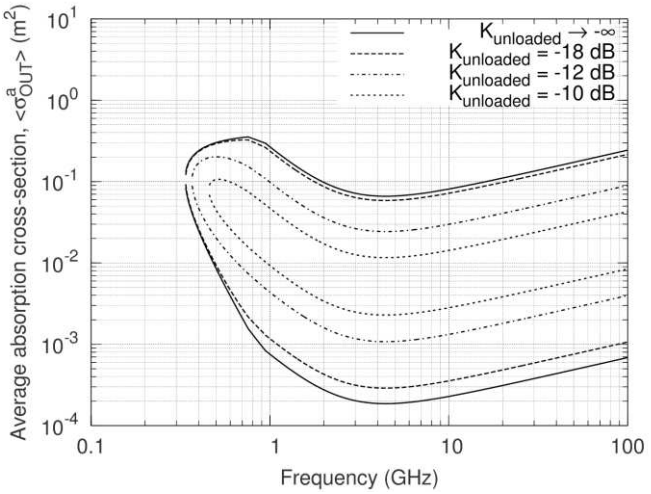

Fig. 10. Estimated boundaries on the ACS of an object for a relative uncertainty of α = 1/3 and various loading dependent K-factors, with b = 2/5, using the semi-empirical model for the chamber Q-factor.

Fig. 10 shows the effect on the 1/3 relative uncertainty bounds of allowing the K-factor to vary with the chamber loading using b = 2/5. As expected, the uncertainty bounds now close in more rapidly with increasing unloaded K-factors. For an unloaded K-factor greater than -8 dB the 1/3 relative uncertainty bounds collapse into each other completely, indicating that the ACS cannot be measured with less than 1/3 relative uncertainty.

The measured Q-factor and unloaded K-factor of the chamber can be included directly in the uncertainty model (with b = 2/5) producing the uncertainty bounds shown in Fig. 11. In this case the number of independent samples has been constrained to that actually obtained in the measurement, rather than the maximum number available based on (9) and (10). These bounds are somewhat different to those predicted by the simple model of the chamber due to the difference between the measured and modeled Q-factor and K-factor displayed in Fig. 6. This result suggests that from a frequency of about 3 GHz upwards, ACS measurements can

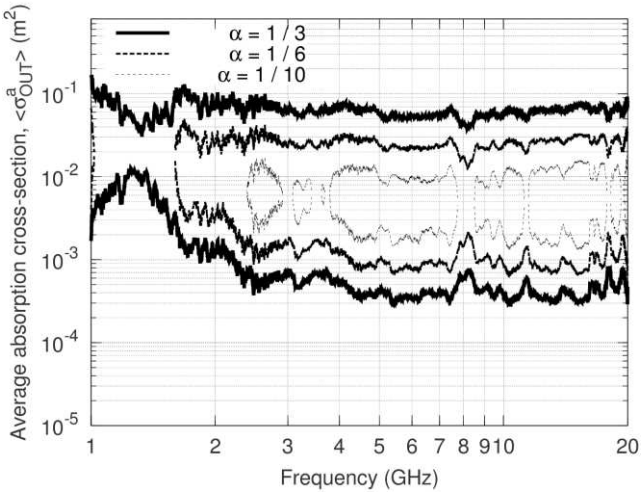

Fig. 11.Estimated boundaries on the ACS of an object for a relative uncertainty of α = 1/3, 1/6 and 1/10 (outer, central and inner boundaries respectively) using the measured unloaded Q-factor and K-factor and taking b = 2/5. The number of independent samples is limited to that taken in the measurement.

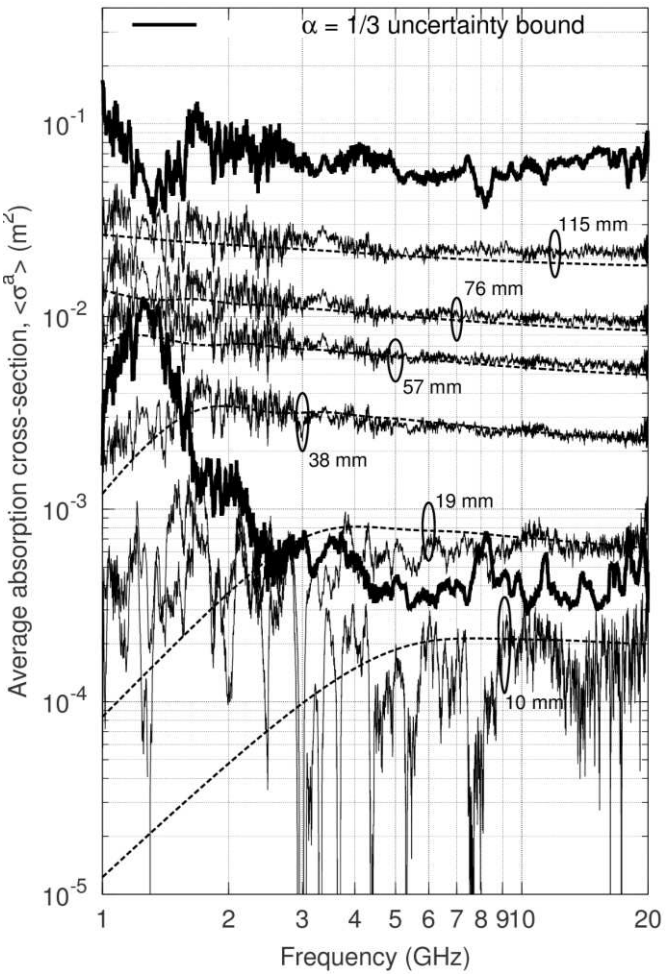

Fig. 12. Measured ACS of the RAM cubes (solid lines) compared to predictions by a Mie Series calculation for spheres of the same surface area (dashed lines). Corresponding lines are circles and labeled by the cube size. The α = 1/3 relative uncertainty bounds on the ACS for the specific measurement parameters are shown as a thick solid lines.

be made over a one decade range with a relative uncertainty of 1/10 and over a two decade range with an uncertainty of 1/3. Below 3 GHz, and especially below 2 GHz, only lower accuracy can be achieved over a more limited range. In practice this chamber is limited to a lowest frequency of about 2 GHz for ACS measurements.

The measured ACSs of the RAM cubes are shown in Fig. 12 compared to the predictions of the Mie Series. The 1/3 relative uncertainty bounds, determined using the measured Q-factor and K-factor, are also shown. Very good agreement between the measurement and Mie Series calculations are obtained when the ACS is within the predicted uncertainty bounds. For the smaller cube the ACS falls below the lower bound and it can be observed that measurement and Mie Series results then diverge.

VII. Conclusions

We have presented an extended uncertainty model which predicts the range of ACS that can be measured within a reverberation chamber of specified geometry within a given uncertainty when stepped mechanical tuning and frequency tuning are used. This provides a practical method to design both reverberation chambers and experiments to achieve optimum accuracy in ACS measurements for a wide range of application including electromagnetic compatibility shielding measurements, human exposure assessment in diffuse environments and material characterization. This has been achieved by extending Carlberg's formula for the uncertainty in reverberation chamber ACS measurements to include the effects of both the chamber loading on the number of independent samples and non-stochastic fields as characterized by the K-factor. The uncertainty formula has been applied to predicting the range of ACS over which ACS measurements can be made with a defined relative uncertainty. The uncertainty model has been validated by measurements on a set of absorbing cubes with different sizes so that their ACSs probe the bounds of measurable ACS in the chamber used.

We have shown that the presence of a non-negligible amount of non-stochastic energy in the chamber, quantified by a K-factor greater than about -12 dB, poses a significant hindrance to accurate ACS measurement. Remley et al have shown that source (position) tuning is effective at reducing the K-factor and therefore offers the prospect of improving the accuracy of ACS measurements in experiments where it is practical [9]. We have also demonstrated that it is difficult to achieve more than a two-decade range in measurable ACS within a single chamber and therefore there is a need to match the chamber to the range of ACS that is being measured.

References

[1] U. Carlberg, P.-S. Kildal, A. Wolfgang, O. Sotoudeh, and C. Orlenius, "Calculated and measured absorption cross sections of lossy objects in reverberation chamber", *IEEE Transactions on Electromagnetic Compatibility*, vol. 46, no. 2, pp. 146–154, May 2004.

[2] A. Gifuni, "On the measurement of the absorption cross section and material reflectivity in a reverberation chamber," *IEEE Transactions on Electromagnetic Compatibility*, vol.51, pp. 1047-1050, November 2009.

[3] I. D. Flintoft, G. C. R. Melia, M. P. Robinson, J. F. Dawson and A. C. Marvin, "Rapid and accurate broadband absorption cross-section measurement of human bodies in a reverberation chamber", *IOP Measurement Science and Technology*, vol. 26, no. 6, pp. 065701, June 2015.

[4] G. C. R. Melia, M. P. Robinson, I. D. Flintoft, A. C. Marvin and J. F. Dawson, "Broadband measurement of absorption cross-section of the human body in a reverberation chamber", *IEEE Transactions on Electromagnetic Compatibility*, vol. 55, no. 6, pp. 1043-1050, December 2013.

[5] P. Hallbjörner, U. Carlberg, K. Madsén and J. Andersson, "Extracting electrical material parameters of electrically large dielectric objects from reverberation chamber measurements of absorption cross section", *IEEE Transactions on Electromagnetic Compatibility*, vol. 47, no. 2, pp. 291-303, May 2005.

[6] I. D. Flintoft, M. P. Robinson, G. C. R. Melia, J. F. Dawson and A. C. Marvin, "Average absorption cross-section of the human body measured at 1-12 GHz in a reverberant environment: Results of a human volunteer study", *IOP Physics in Medicine and Biology*, vol. 59, no. 13, pp. 3297-3317, July 2014.

[7] A. Bamba, D. P. Gaillot, E. Tanghe, G. Vermeeren, W. Joseph, M. Lienard and L. Martens, "Assessing whole-body absorption cross section for diffuse exposure from reverberation chamber measurements", *IEEE Transactions on Electromagnetic Compatibility*, vol.57, no.1, pp.27,34, February 2015.

[8] D. A. Hill, M. T. Ma, A. R. Ondrejka, B. F. Riddle, M. L. Crawford and R. T. Johnk, "Aperture excitation of electrically large, lossy cavities", *IEEE Transactions on Electromagnetic Compatibility*, vol. 36, no. 3, pp.169-178, August 1994.

[9] K. A. Remley, R. J. Pirkl, H. A. Shah and C.-M Wang, "Uncertainty from choice of mode-stirring technique in reverberation chamber measurements", *IEEE Transactions on Electromagnetic Compatibility*, vol. 55, no. 6, pp. 1022-1030, December 2013.

[10] C. L. Holloway, H. A. Shah, R. J. Pirkl, W. F. Young, D. A. Hill and J. M. Ladbury, "Reverberation chamber techniques for determining the radiation and total efficiency of antennas," *IEEE Transactionson Antennas and Propagation*, vol. 60, pp. 1758-1770, April 2012.

[11] J. G. Kostas and B. Boverie, "Statistical model for a mode-stirred chamber", *IEEE Transactions on Electromagnetic Compatibility*, vol. 33, no. 4, pp. 366-370, November 1991.

[12] P. Hallbjörner, "A model for the number of independent samples in reverberation chambers", *Microwave and Optical Technology Letters*, vol. 33, no. 1, pp. 25-28, April 2002.

[13] K. Madsén, P. Hallbjörner and C. Orlenius, "Models for the number of independent samples in reverberation chamber measurements with mechanical, frequency, and combined stirring", *IEEE Antennas and Wireless Propagation Letters*, vol. 3, no. 1, pp. 48-51, December 2004.

[14] N. Wellander, O. Lunden and M. Backstrom, "Experimental investigation and mathematical modeling of design parameters for efficient stirrers in mode-stirred reverberation chambers", *IEEE Transactions on Electromagnetic Compatibility*, vol. 49, no. 1, pp. 94 - 103, February 2007.

[15] C. L. Holloway, D. A. Hill, J. M. Ladbury, P. F. Wilson, G. Koepke and J. Coder, "On the use of reverberation chambers to simulate a Rician radio environment for the testing of wireless devices",*IEEE Transactions on Antennas and Propagation*, vol. 54, no. 11, pp. 3167-3177, November 2006.

[16] S. van de Beek, K. A. Remley, C. L. Holloway, J. M. Ladbury and F. Leferink, "Characterizing large-form-factor devices in a reverberation chamber", International Symposium on Electromagnetic Compatibility (EMC EUROPE) 2013, pp. 375-380, 2-6 Sept. 2013.

[17] Emerson & Cuming, "Eccosorb LS", Technical Bulletin, Revision 5/11/07, URL: http://www.eccosorb.com/Collateral/Documents/English-US/LS.pdf.

[18] E. Le Ru and P. Etchegoin, SERS and Plasmonics Codes (SPlaC), Victoria University of Wellington, New Zealand, 2006. URL: http://www.victoria.ac.nz/raman/book/codes.aspx.

[19] T. G. Tang, Q. M. Tieng and M. W. Gunn, "Equivalent circuit of a dipole antenna using frequency independent lumped elements", *IEEE Transactions on Antennas and Propagation*, vol. 41, no. 1, pp. 100-103, January 1993.